RSC Advances

ROYAL SOCIETY OF CHEMISTRY

www.rsc.org/advances

Graphical abstract

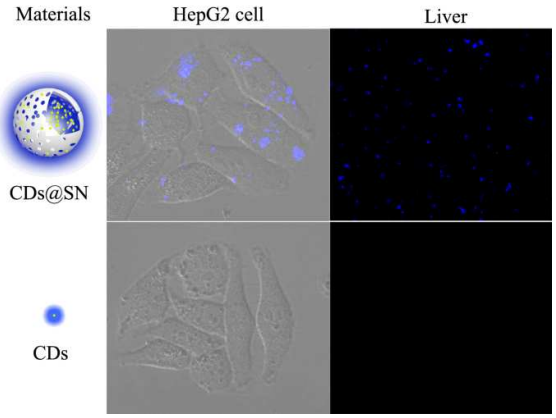

Carbon dots embedded in silica nanorattle (CDs@SN) nanocomposites with highly luminescence are synthesized and exhibit brighter fluorescence *in vitro* and *in vivo* than CDs alone.

Journal Name

RSCPublishing

ARTICLE

Facile synthesis of highly luminenscent carbon dots@silica nanorattle for *in vivo* bioimaging

Cite this: DOI: 10.1039/xoxxooooox

Changhui Fu, Li Qiang, Qinghua Liang, Xue Chen, Linlin Li, Huiyu Liu, Longfei Tan, Tianlong Liu, Xianling Ren, Xianwei Meng*

Received ooth January 2012,
Accepted ooth January 2012

DOI: 10.1039/xoxxooooox

www.rsc.org/

Owing to their many advantages including the chemical inertness, low toxicity, and stable photoluminescence, carbon dots (CDs) have been considered as one of the rising fluorescent materials in the field of bio-labeling. Despite many burgeoning achievements in optical cell imaging, the exploration of multifunctional CDs for *in vivo* imaging and potential biotherapy is still a great challenge. In this work, carbon dots embedded in silica nanorattle (CDs@SN) nanocomposites exhibiting strong luminescence was prepared via a facile hydrothermal method. The structure and optical properties of the resultant CDs@SN were well studied by Fourier transform infrared (FT-IR) spectrum, transmission electron microscopy (TEM), and photoluminescence. The resultant CDs@SN was used for *in vitro* cell labeling and *in vivo* bioimaging, and exhibits a higher cellular uptake and brighter fluorescence than CDs alone. Furthermore, the CDs@SN shows excellent biocompatibility with the HepG2 and red blood cells. We deem that combining the outstanding properties of SNs with CDs would further promote the development of CDs in the biological applications, especially achieving multifunctional CDs with targeting, *in vivo* imaging and therapeutic-delivery capabilities.

Introduction

Fluorescence detection technology is widely used in the fields of biomedicine and detection.[1, 2] Particularly, the emerging nanotheranostics play an important role in achieving the imaging-guided tumor-specific drug delivery with the assistance of imaging molecules, and also shows great potential in rapid developing personalized medicine that enable to integrate the therapeutic molecules and imaging agents.[3, 4] As such, the imaging agent is one of the most important components for nanotheranostics. Compared with the traditional fluorescent dye and semiconductor quantum dots based on metal chalcogenides, fluorescent carbon dots (CDs) have attracted increasing interest owing to their eco-friendly and low-cost precursor, good biocompatibility, high hydrophilicity and low photo-bleaching.[5-7] Hence, CDs have become promising candidates in the field of bioimaging.[7-10] Recently, many strategies like choosing different precursors and doping with other heteroatoms have been developed for improving the optical properties to achieve the biological activities of CDs. [5,11,8] For example, CDs with a high fluorescence quantum yield of 80% were prepared by hydrothermal treatment of citric acid and ethylenediamine.[10] The CDs prepared from fresh tender ginger showed a higher selectivity inhibition towards HepG2 cells.[8] N-doped or Si-doped CDs not only improves the fluorescent property but also provides more active sites to expand their application. [11-13] Despite these encouraging achievements, further synthesis and investigation on multifunctional CDs is desirable to expand their applications for *in vivo* bioimaging, biosensing, and even the diagnosis and treatment of human disease. [8]

As well known, the highly luminescent CDs are usually smaller than 10 nm. However, previous studies have demonstrated that the nanoparticles with the size of smaller than 10 nm have a short retention time *in vivo* because they would be rapidly eliminated from the body along with the urine excretion.[14-16] The suitable size of the nanoparticles for the passive tumor uptake is about 60-400 nm in the tumor delivery due to their longer retention time in the tumor and improved therapeutic efficacy.[17, 18] On the other hand, CDs are often free of porous structure and have a small specific surface area. As a result, it is impossible to directly use the CDs as nanotheranostics in cancer therapy *in vivo* for their short retention time and difficulty for drug loading. In order to solve these problems, a promising strategy may be practicable by combining the CDs with other biocompatible materials like gold nanorod and graphene oxide while keeping their highly luminescence and other intrinsic merits.[19, 20] However, these CDs based compounds can be only used for imaging *in vitro*. As a result, it is urgent to extent the application of CD

compounds for imaging *in vivo* because the extremely different environment between *in vivo* and *in vitro*.[21-23]

Mesoporous nanosilica is one of the most investigated nanomaterials for cancer therapy as well as delivery of therapeutic payloads owing to their excellent stability, good biocompatibility, and easy modification. In recent years, our group has made much process in the construction of mesoporous silica for biological applications. We have synthesized silica nanorattles (SNs) with unique hollow and mesoporous shell,[24] and also achieved the growth of Au and Fe_3O_4 nanoparticles in the cavity of the SN.[25, 26] Furthermore, our previous studies demonstrated that the SN is one kind of ideal promising new-generation drug delivery systems with possessing sustained release property, high drug loading capacity, high therapy efficacy and low systematic toxicity *in vivo*.[3, 21, 22, 27-30] Therefore, it can be imaged that combining the outstanding properties of SNs with CDs may further promote the development of CDs and SNs in the biological applications, especially achieving multifunctional CDs with targeting, *in vivo* imaging and therapeutic-delivery capabilities.[7, 27]

In this study, the carbon dots embedded in the silica nanorattle (CDs@SN) has been synthesized in a facile hydrothermal method. The resultant CDs@SN shows fluorescence and higher cell uptake than CDs obtained in a sample way. Moreover, the CDs@SN can be used for *in vitro* cell labeling and *in vivo* bioimaging, and shows excellent biocompatibility.

Results and discussion

The CDs@SN was prepared by in-situ growth of CDs in the cavity of SN through a hydrothermal treatment of the impregnated SN with citric acid and ethanediamine. As we know, highly luminescent CDs can be synthesized by hydrothermal treating the aqueous solution of citric acid and ethylenediamine.[10] Owing to the mesoporous structure and hydrophilcity of SN, the citric acid and ethylenediamine can be easily introduced into the inner cavity of SN with the assistance of sonication under vacuum. As a result, the subsequent hydrothermal treatment at 200 ℃ for 8 h could result in the in stiu formation of CDs inside of the SN. Moreover, the as-formed CDs could not get out from SN due to the small pore size of shell. Then, the CDs@SN was obtained.

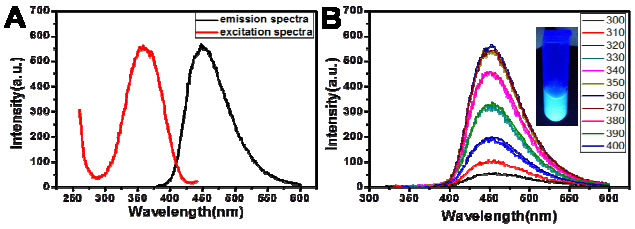

Fig. 1 (A) The PL spectra and (B) the emission spectra excited with different wavelength of the CDs@SN.

The fluorescent property of the CDs@SN is firstly studied by photoluminescence (PL). A maximum emission at 450 nm is observed under an excitation of 350 nm (Fig. 1A). The maximum emission of the CDs@SN shows little change as the excitation wavelength changed from 300 to 400 nm (Fig. 1B). Furthermore, the aqueous solution of the CDs@SN exhibits bright blue fluoresence under UV light (inset in Fig. 1B), suggesting the presence of CDs in CDs@SN.[31] The PL quantum yield of the as-obtained CDs is about 55 %. As shown in Fig. 1S, though the PL life time of CDs@SN (9.61 ns) is significantly different from that of CDs alone (15.64 ns), suggesting the existence of chemical interaction between CDs and SN in CDs@SN, it is comparable to that of other CDs and CDs-based composites in the previous reported.[32]

Transmission Electron Microscope (TEM) is further used to confirm the location of CDs in the CDs@SN. Low magnified TEM image shows that the structure of SN has negligible alternation after hydrothermal treatment for its excellent thermal and mechanical stabilities (Fig. 2A). As can be seen from the high resolution TEM image in Fig. 2B, many tiny dark CDs can be clearly observed in the cavity of SN in the CDs@SN compared with the SN alone (Fig. S1B). The average size of the CDs is about 8 nm based on the statistical analysis of more than five hundred particles using the ImageJ software (Fig. 2D). Furthermore, a slight increase of the shell thickness of the CDs@SN indicates that some CDs located at the surface of SN (Fig. S1). However, negligible change of the Zeta potential was observed between the SN and CD@SN (Fig. 2C and S2).

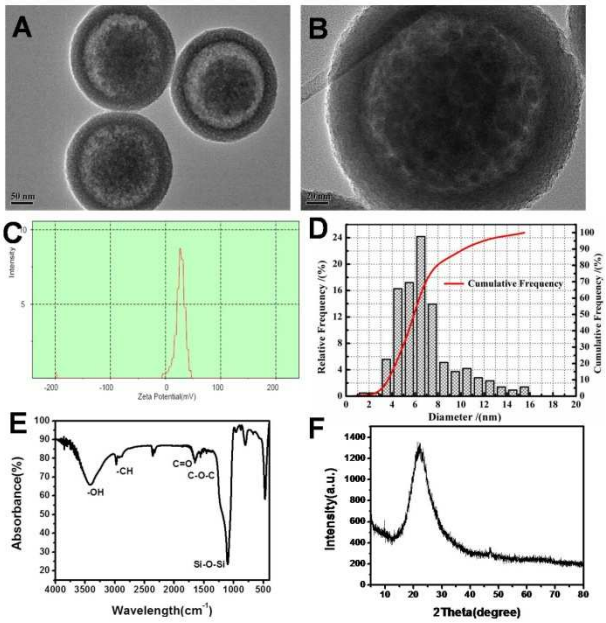

Fig. 2 (A-B) Low and high-magnified TEM images and (C) the zeta of the CDs@SN, (D) the diameter distribution of the CDs in the CDs@SNs, (E) the FT-IR spectrum and (F) the XRD pattern of the resultant CDs@SN.

In order to confirm the presence of CDs in CDs@SN, FT-IR spectrum is performed in detail. Both the SN and CDs@SN exhibit a strong stretching vibration band of Si-O at 1095 cm^{-1} and a stretching vibration band of O–H with a broad peak at 3500 cm^{-1} (Fig. 2E and Fig. S1). Also C=O at 1630 cm^{-1}, and C–C at 1430 cm^{-1} are observed in the SN and CDs@SN. Furthermore, the CDs@SN shows a characteristic absorption of stretching vibration bands of C–H at 2950 cm^{-1}, indicating the

presence of CDs in the CDs@SN.[6 9] The reason for the weak peak corresponding to CDs may be that the CDs lied in the cavity of SN more than that at the surface of SN. The chemical composition of CDs@SN nanocomposites were further characterized by SEM combined with EDS analysis. As shown in Fig. S2, Si, O and C elements were found in CDs@SN and SN. Moreover, the contents of C and O in CDs@SN were higher than those in SN, indicating the presence of CDs in CDs@SN. Due to the amorphous structures of SN and the CDs, the XRD profiles exhibit a broad diffraction peak from 20 to 30° (Figs. 2F and S1).

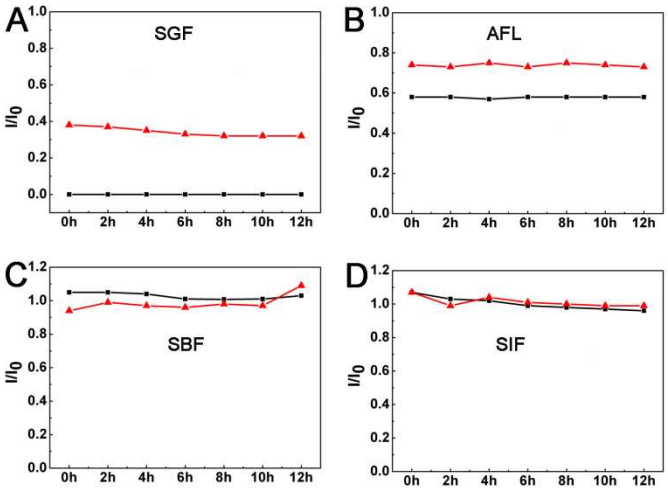

Fig. 3 The PL change of the CDs@SN and CDs in different simulation medium (black square: CDs; red triangle: CDs@SN).

For practical applications in biological system, the luminescence of CDs@SN should be stable in a wide range of electrolyte concentrations such as *in vivo* media where the ionic concentration is known to be the complexity. Afterwards, we study the effects of simulated biomedium on the fluorescent intensity of CDs@SN and CDs by exposing them to stimulated gastric fluid (SIF), fasted-state simulated intestinal fluid (SGF), artificial lusosomal fluid (AFL) and simulated body fluid (SBF) for different time intervals. As can be seen in Fig. 3A, nearly no fluorescence of CDs is observed in the SGF (pH 1.6). However, the CDs@SN dispersed in the SGF still show 40% fluorescent intensity of that dispersed in PBS, indicating that the SN significantly protected the CDs from fluorescence quench in the SGF. Furthermore, a much stronger emission of the CDs@SN in the AFL (pH 5.4) is observed than that of CDs in the AFL (Fig. 3B). No remarkable changes of the fluorescent intensity of CDs or CDs@SN are observed when they are dispersed in the SBF (pH 7.2) and SIF (pH 6.5), as shown in Figs. 3C and 3D. These results confirm that the CDs@SN shows more stable fluorescence than that of CDs alone.

In order to explore the capability of CDs@SN for intracellular imaging, CDs@SN was used for *in vitro* bioimaging by incubating HepG2 with CDs@SN at a low concentration of 50 μg mL^{-1}. After exposure for 8 h, bright fluorescent signal is observed in the cytoplasm of the cells, indicating that CDs@SN can be quickly uptake by living cells (Fig. 4A-B). In contrast, almost invisible fluorescence is detected in the cells incubated with CDs alone performed in a similar experimental condition (Fig. 4C-D), suggesting that the CDs@SN exhibits a better staining ability than that of CDs. Moreover, it is also found that the location of fluorescent signal of CDs@SN in the cells is dispersive, which is very different from that of the reported CDs that was homogeneous.[5, 8] The reason may be the different uptake mechanism of CDs@SN caused by different physicochemical properties. Furthermore, flow cytometry is used to quantificationally analyze the fluorescent intensity of HepG2 uptake of CDs@SN and CDs. As shown in Fig. 4(E-H), the fluorescent intensity of HepG2 treated by CDs@SN is near 10 times than that of HepG2 treated by CDs, agreeing well with the results observed by confocal optical microscopy.

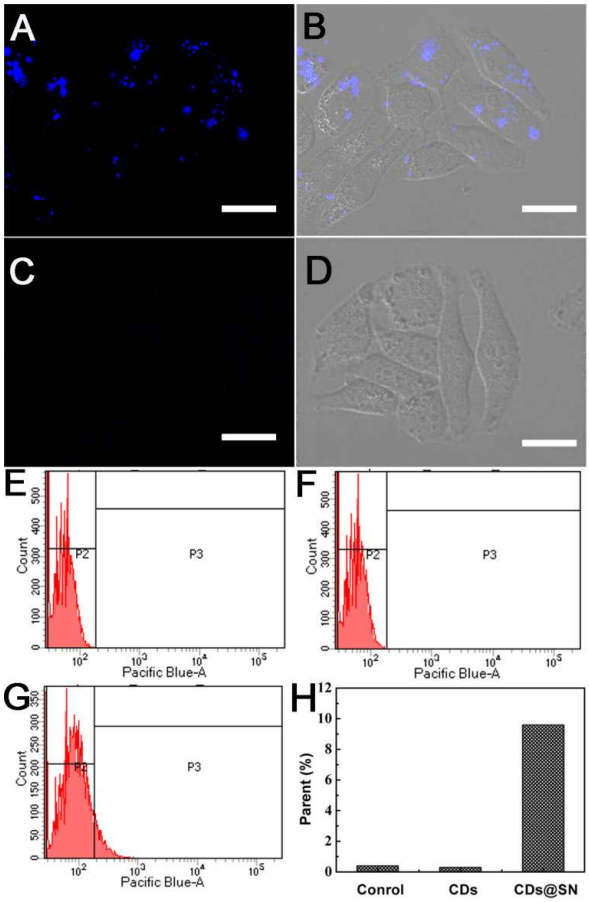

Fig. 4 Confocal optical images of HepG2 cells treated with CDs@SN (A-B) and CDs (C-D). A and C were obtained under UV light. B and D were obtained under bright light. Flow cytometry analysis of the fluorescent intensity in the cells incubated with the control group (E), CDs (F), and CDs@SN (G). H is the corresponding fluorescent intensity expressed as percentages. The scale bar is 20 μm.

Although fluorescent CDs have been widely used for cell imaging *in virto,* few works were involved *in vivo* imaging. [19, 20, 33] To further probe the effectiveness of the CDs@SN act as optical marker *in vivo*, we employed the frozen section of

tissues to visualize the fluorescence of the normal mice administrated with CDs@SN. As shown in Fig. 5 and S3, no fluorescence is observed in the liver, spleen and kidney after injection the mice with CDs for 1, 4 and 12 h through vein, which may be attributed to the quick excretion from the body of the CDs and the existence of fluorescent quenching agents in the bio-medium. In contrast, strong blue fluorescence is detected in the liver, spleen and kidney of the mice intravenously injected with CDs@SN for 1, 4 and 12 h. Furthermore, it is found that the bright fluorescence signal is detected in the H22 tumor after intratumoral injection with CDs@SN, as shown in Fig. 6. These results confirm that the CDs@SN can be used for *in vivo* imaging and shows great potential application in biomedicine. The CDs@SN used as nanotheranostics is under way.

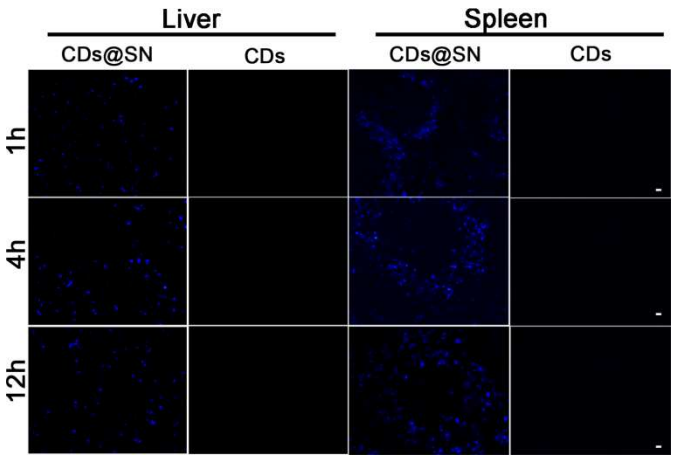

Fig. 5 The frozen section of liver and spleen from the mice administrated with CDs@SN and CDs after intravenous injection at different interval. The scale bars denote 20 μm.

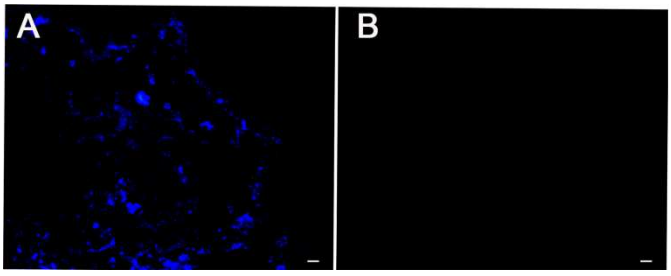

Fig. 6 The frozen section of tumor from the mice administrated with CDs@SN and the control group after intratumoral injection. The scale bars is 20 μm.

Low cytotoxicity is necessary for ideal multifunctional biomaterials applied for bioimaging. Hence, we evaluate the cytotoxicity of the CDs@SN by using the HepG2 with WST-1 assay and calcein-AM/PI staining method. As shown in Fig. 7A, the relative cell viability is over 85% after exposure with the CDs@SN even at the concentration of 250 μg mL^{-1} for 24 h and 48 h, suggesting the excellent biocompatibility of the CDs@SN. The calcein-AM/PI staining also reveals strong green fluorescence, which is indicative of live cells, in the entire field of vision. No red fluorescence representing the dead cells are observed after exposing HepG2 cells with CDs@SN for 48 h, as shown in Fig. 7C and 7D. Moreover, it is found that the hemolysis rate of the CDs@SN at 800 and 600 μg mL^{-1} is about 2%, which is much less than the upper limited value of hemolysis index (5%), indicating that no hemolysis happened after intravenous administration of the CDs@SN (Fig. 7B and S4). All these results confirm the good biocompatibility of the CDs@SN.

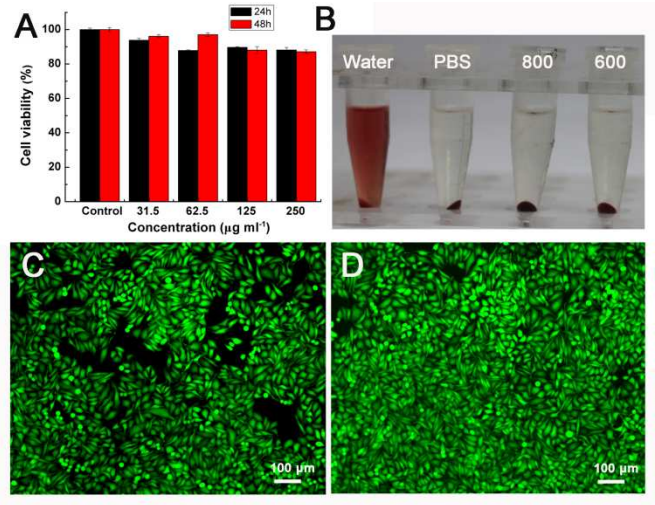

Fig. 7 The cytotoxic evaluation of the CDs@SN on the HepG2 cells with WST-1 assay (A) and calcein-AM/PI staining (C-D) methods, C represents the HepG2 cells treated with the CDs@SN and D represents the control group. B is the photo of red blood cell after adding CDs@SN at 800 and 600 μg mL^{-1}.

Conclusion

In conclusion, highly luminescent and biocompatible carbon dots@silica nanoratte (CDs@SN) nanocomposite involving the presence of CDs in the interior of silica nanorattle was synthesized via a simple hydrothermal method. The combination of SN not only protects the CDs from fluorescence quenching but also makes the CDs have a long retention time in organs. Consequently, the CDs@SN can be effectively used for *in vitro* cell labeling and *in vivo* bioimaging. We believe the highly luminescent and good biocompatible CDs@SN with unique mesoporous and hollow structure shows great potential application in biomedicine as nanotheranostics.

Acknowledgements

This work was supported by the National Natural Science Foundation of China (Nos. 31400854, 61171049, 31270022, 31271075, 51302274, 51202260, 81201814 and 81471784) and National Hi-Tech. Research and Development Program of China (Nos. 2013AA032201 and 2012AA022701).

Notes and references

Laboratory of Controllable Preparation and Application of Nanomaterials, Center for Micro/nanomaterials and Technology, Technical Institute of Physics and Chemistry, Chinese Academy of Sciences, Beijing 100190, China. Fax: 8610 62554670; Tel: 86 10 82543521; E-mail: mengxw@mail.ipc.ac.cn

† Footnotes should appear here. These might include comments relevant to but not central to the matter under discussion, limited experimental and spectral data, and crystallographic data.
Electronic Supplementary Information (ESI) available: [details of any supplementary information available should be included here]. See DOI: 10.1039/b000000x/

1. J. F. Wei, J. Ren, J. Liu, X. W. Meng, X. L. Ren, Z. Z. Chen and F. Q. Tang, *Biosens. Bioelectron*, 2014, **52**, 304-309.
2. J. F. Wei, L. Qiang, J. Ren, X. L. Ren, F. Q. Tang and X. W. Meng, *Anal. Methods-Uk*, 2014, **6**, 1922-1927.
3. F. Gao, L. Li, C. Fu, L. Nie, D. Chen and F. Tang, *Adv Mater*, 2013, **25**, 5508-5513.
4. D.-E. Lee, H. Koo, I.-C. Sun, J. H. Ryu, K. Kim and I. C. Kwon, *Chem. Soc. Rev.*, 2012, **41**, 2656-2672.
5. C. Shen, Y. Sun, J. Wang and Y. Lu, *Nanoscale*, 2014, **6**, 9139-9147.
6. Q. Liang, W. Ma, Y. Shi, Z. Li and X. Yang, *Carbon*, 2013, **60**, 421-428.
7. C. Q. Ding, A. W. Zhu and Y. Tian, *Accounts Chem. Res.*, 2014, **47**, 20-30.
8. C.-L. Li, C.-M. Ou, C.-C. Huang, W.-C. Wu, Y.-P. Chen, T.-E. Lin, L.-C. Ho, C.-W. Wang, C.-C. Shih, H.-C. Zhou, Y.-C. Lee, W.-F. Tzeng, T.-J. Chiou, S.-T. Chu, J. Cang and H.-T. Chang, *J. Mater. Chem. B*, 2014, **2**, 4564-4571.
9. J. Wang, C.-F. Wang and S. Chen, *Angew. Chem. Int. Ed.*, 2012, **124**, 9431-9435.
10. S. Zhu, Q. Meng, L. Wang, J. Zhang, Y. Song, H. Jin, K. Zhang, H. Sun, H. Wang and B. Yang, *Angew. Chem. Int. Ed.,* 2013, **52**, 3953-3957.
11. Z. Qian, X. Shan, L. Chai, J. Ma, J. Chen and H. Feng, *ACS Appl. Mater. Inter.*, 2014, **6**, 6797-6805.
12. Z. Qian, J. Ma, X. Shan, H. Feng, L. Shao and J. Chen, *Chem. –Eur. J.*, 2014, **20**, 2254-2263.
13. Z. Qian, J. Ma, X. Shan, L. Shao, J. Zhou, J. Chen and H. Feng, *RSC Advances*, 2013, **3**, 14571-14579.
14. S. T. Yang, L. Cao, P. G. J. Luo, F. S. Lu, X. Wang, H. F. Wang, M. J. Meziani, Y. F. Liu, G. Qi and Y. P. Sun, *J. Am. Chem. Soc.*, 2009, **131**, 11308-11309.
15. X. L. Huang, F. Zhang, L. Zhu, K. Y. Choi, N. Guo, J. X. Guo, K. Tackett, P. Anilkumar, G. Liu, Q. M. Quan, H. S. Choi, G. Niu, Y. P. Sun, S. Lee and X. Y. Chen, *ACS Nano*, 2013, **7**, 5684-5693.
16. H. S. Choi, W. Liu, P. Misra, E. Tanaka, J. P. Zimmer, B. I. Ipe, M. G. Bawendi and J. V. Frangioni, *Nat. Biotechnol.*, 2007, **25**, 1165-1170.
17. H. Liu, T. Liu, L. Li, N. Hao, L. Tan, X. Meng, J. Ren, D. Chen and F. Tang, *Nanoscale*, 2012, **4**, 3523-3529.
18. Y. Gao, Y. Wang, A. Fu, W. Shi, D. Yeo, K. Q. Luo, H. Ow and C. Xu, *J. Mater. Chem. B*, 2015, **3**, 1245-1253.
19. K. K. Datta, O. Kozak, V. Ranc, M. Havrdova, A. B. Bourlinos, K. Safarova, K. Hola, K. Tomankova, G. Zoppellaro, M. Otyepka and R. Zboril, *Chem. Commun.*, 2014, **50**, 10782-10785.
20. S. Pandey, M. Thakur, A. Mewada, D. Anjarlekar, N. Mishra and M. Sharon, *J. Mater. Chem. B*, 2013, **1**, 4972-4982.
21. L. Li, F. Tang, H. Liu, T. Liu, N. Hao, D. Chen, X. Teng and J. He, *ACS Nano*, 2010, **4**, 6874-6882.
22. F. Gao, L. Li, T. Liu, N. Hao, H. Liu, L. Tan, H. Li, X. Huang, B. Peng, C. Yan, L. Yang, X. Wu, D. Chen and F. Tang, *Nanoscale*, 2012, **4**, 3365-3372.
23. H. C. Fischer and W. C. W. Chan, *Curr. Opin. Biotech.*, 2007, **18**, 565-571.
24. D. Chen, L. Li, F. Tang and S. Qi, *Adv. Mater.*, 2009, **21**, 3804-3807.
25. L. Tan, D. Chen, H. Liu and F. Tang, *Adv Mater*, 2010, 22, 4885-4889.
26. L. Qiang, X. Meng, L. Li, D. Chen, X. Ren, H. Liu, J. Ren, C. Fu, T. Liu, F. Gao, Y. Zhang and F. Tang, *Chem. Commun.*, 2013, **49**, 7902-7904.
27. F. Tang, L. Li and D. Chen, *Adv Mater*, 2012, **24**, 1504-1534.
28. T. Liu, L. Li, X. Teng, X. Huang, H. Liu, D. Chen, J. Ren, J. He and F. Tang, *Biomaterials*, 2011, **32**, 1657-1668.
29. L. Li, Y. Guan, H. Liu, N. Hao, T. Liu, X. Meng, C. Fu, Y. Li, Q. Qu, Y. Zhang, S. Ji, L. Chen, D. Chen and F. Tang, *ACS Nano*, 2011, **5**, 7462-7470.

30. C. Fu, T. Liu, L. Li, H. Liu, D. Chen and F. Tang, *Biomaterials*, 2013, **34**, 2565-2575.

31. Y. Dong, J. Shao, C. Chen, H. Li, R. Wang, Y. Chi, X. Lin and G. Chen, *Carbon*, 2012, **50**, 4738-4743.

32. C. W. Lai, Y. H. Hsiao, Y. K. Peng and P. T. Chou, *J. Mater. Chem.*, 2012, **22**, 14403-14409.

33. H. T. Shi, J. F. Wei, L. Qiang, X. Chen and X. W. Meng, *J. Biomed. Nanotechnol.*, 2014, **10**, 2677-2699.

